

Unlimited Sampling of Bandpass Signals: Computational Demodulation via Undersampling

Gal Shtendel, Dorian Florescu, and Ayush Bhandari

CONTENTS

I	Introduction	3
II	Signal Folding Architectures	6
II-A	Ideal Modulo Folding (\mathcal{M}_λ)	6
II-B	Generalized Modulo Nonlinearity ($\mathcal{M}_\mathbf{H}$)	7
II-C	Non-Ideal Modulo Folding ($\widetilde{\mathcal{M}}_\lambda$)	8
III	Towards Computational Demodulation via Modulo Undersampling	9
III-A	Undersampling with the Ideal Modulo Architecture	10
III-B	Undersampling with Generalized Modulo Architecture	14
III-C	Fourier-Domain Approach for Modulo Undersampling	14
IV	Experiments	18
IV-A	Numerical Simulations	18
IV-B	Hardware Experiments	20
V	Conclusions and Future Work	21
	References	23

arXiv:2307.04917v1 [cs.IT] 10 Jul 2023

This work is supported by the UK Research and Innovation council’s *Future Leaders Fellowship* program “Sensing Beyond Barriers” (MRC Fellowship award no. MR/S034897/1). Project page for (future) release of hardware design, code and data: <https://bit.ly/USF-Link>.

The authors are with the Dept. of Electrical and Electronic Engineering, Imperial College London, South Kensington, London SW7 2AZ, UK. (Email: {g.shtendel21,d.florescu,a.bhandari}@imperial.ac.uk or ayush@alum.mit.edu).

Manuscript Submitted: 20XX.

Abstract

Bandpass signals are an important sub-class of bandlimited signals that naturally arise in a number of application areas but their high-frequency content poses an acquisition challenge. Consequently, “Bandpass Sampling Theory” has been investigated and applied in the literature. In this paper, we consider the problem of modulo sampling of bandpass signals with the main goal of sampling and recovery of high dynamic range inputs. Our work is inspired by the Unlimited Sensing Framework (USF). In the USF, the modulo operation folds high dynamic range inputs into low dynamic range, modulo samples. This fundamentally avoids signal clipping. Given that the output of the modulo nonlinearity is non-bandlimited, bandpass sampling conditions never hold true. Yet, we show that bandpass signals can be recovered from a modulo representation despite the inevitable aliasing. Our main contribution includes proof of sampling theorems for recovery of bandpass signals from an undersampled representation, reaching sub-Nyquist sampling rates. On the recovery front, by considering both time- and frequency-domain perspectives, we provide a holistic view of the modulo bandpass sampling problem. On the hardware front, we include ideal, non-ideal and generalized modulo folding architectures that arise in the hardware implementation of modulo analog-to-digital converters. Numerical simulations corroborate our theoretical results. Bridging the theory–practice gap, we validate our results using hardware experiments, thus demonstrating the practical effectiveness of our methods.

Index Terms

Analog-to-digital conversion (ADC), approximation, bandpass sampling, modulo, Shannon sampling theory.

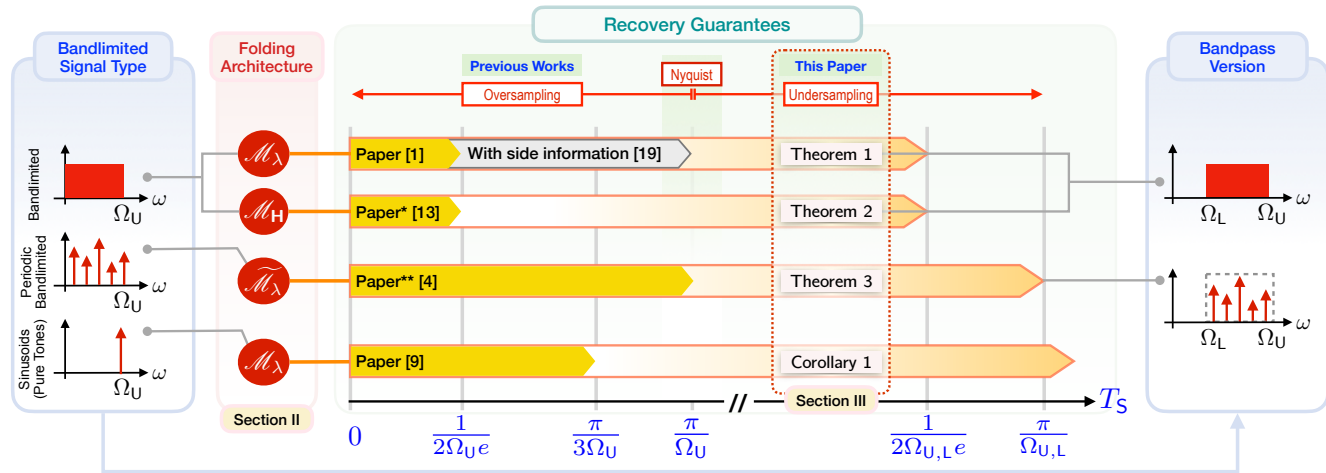


Fig. 1. Summary of recovery guarantees for commonly occurring types of bandlimited signals in the context of unlimited sensing framework (USF) together with different folding architectures denoted by $\mathcal{M}_\lambda, \mathcal{M}_\lambda, \mathcal{M}_H$. We also summarize our contributions in terms of extending the results for bandlimited signal type to their corresponding bandpass case, especially in the undersampled regime.

I. INTRODUCTION

DIGITAL signal acquisition methodology is the workhorse of all modern world electronic systems. This technology is pivoted on Shannon’s Sampling Framework wherein point-wise samples are digitized using the so-called analog-to-digital converter or the ADC. For the theory and practice to work in perfect tandem, it is imperative that the input signal’s dynamic range is matched to the ADC’s dynamic range. When this is not the case, even in noiseless conditions, the resulting samples are distorted due to saturation or clipping. Such a scenario leading to permanent loss of information poses a fundamental bottleneck in all digital systems.

To overcome this bottleneck, the **Unlimited Sensing Framework (USF)** [1]–[6] has been recently proposed as an alternative digital acquisition technology. Unlike previous sampling approaches where *hardware* and *reconstruction algorithms* were mostly decoupled, the USF is pivoted on the theme of *computational sensing* [7] as it harnesses a co-design of hardware and algorithms. In particular,

- **Encoding.** Signal folding¹ is implemented in the hardware pipeline so that any arbitrary high-dynamic-range (HDR), continuous-time input is folded or wrapped within the dynamic range of the ADC. This results in low-dynamic-range samples and entails that signal clipping or saturation problem is eliminated in the encoding stage.
- **Decoding.** Given folded samples, the input HDR signal is mathematically *unfolded* using recovery algorithms. To this end, one of the first recovery guarantees was provided in [1], [3]. It was shown that bandlimited signals can be recovered from a constant factor oversampling of modulo samples with a sampling rate that is independent of the threshold λ . We refer to Fig. 1 for a summary of known recovery rates for different bandlimited signal types [1], [3], [4], [8], [9].

To validate the practical utility of the USF, we have implemented signal folding in hardware using different non-linearities including

¹To get a sense of the hardware functionality of the modulo ADCs built in [4], we refer the reader to the live YouTube demonstration for (a) Sinusoidal Waveform <https://youtu.be/JuZg80gUr8M> and (b) Arbitrary Bandlimited Waveform <https://youtu.be/prV40WlzhH4>.

- Modulo ADCs [4], [5], [10]–[12],
- Generalized Modulo ADCs [13]–[15], as well as,
- Time-Encoding Architectures [6], [16], [17].

Let $\lambda > 0$ denote the saturation threshold of the modulo ADC (\mathcal{M} -ADC). Hardware experiments [4] have established that inputs as large as 25λ to 30λ can be recovered in the presence of non-idealities, system noise and quantization. This was achieved by a Fourier-domain recovery algorithm referred to as the *Fourier-Prony* or US-FP method. The US-FP method is a) non-iterative, b) agnostic to λ , c) operates at the tightest possible sampling rates, and d) is empirically robust to system noise [4], [5] and outliers [10], thus making it particularly attractive for real-world experiments. For theoretical guarantees in the case of noise for the nonideal scenario, the generalized modulo ADC and associated sampling model introduce an additional parameter called *hysteresis* which was used in the context of uniform sampling [13] and time encoding [6].

Related Work on Unlimited Sampling. Several follow-up papers, summarised below, have adopted the USF strategy for modulo sensing and reconstruction *e.g.* [18]–[26], predominantly focused on bandlimited signals (barring [5], [27])

Previous research on bandlimited signals on a real line [1], [3], periodic² bandlimited signals [4] and sinusoidal tones [9] (see Fig. 1). Ordentlich *et al.* studied modulo sampling via rate-distortion theory [18], and also proposed a recovery method [19] assuming a number of unfolded samples known *a priori*. Gong *et al.* [24] proposed a multi-channel method with complex-valued moduli to recover HDR inputs. Azar *et al.* [25] extended the Fourier-Prony approach [4] with additional time-domain constraints. A robust algorithm based on optimization was presented in [28] which was validated via hardware experiments.

Motivation for Bandpass Sampling Theory. The topic of *Bandpass Sampling* has been studied in detail from the perspective of sampling theory *e.g.* [29]–[31] as well as application-centric contexts, *e.g.* sonar [32], [33], radar systems [34], [35], ultrasound imaging [36] and optics [37], [38].

Since bandpass functions are also bandlimited, a natural first thought is to sample them at their Nyquist rate. However, this requires the ADC to operate at very high sampling rates [30], which causes implementation challenges and imply higher power consumption in the ADC [31]. Furthermore, this simplistic view does not leverage the fact that a bandpass signal contains no information in the lowpass region.

—*Existing Strategies for Bandpass Sampling.* Researchers developed the following strategies for efficient acquisition.

- Hardware-only approaches [39] use mixers to demodulate the signal so that it is concentrated in the baseband region. This leads to lower sampling rates but results in complex and more expensive hardware implementation [31].
- Algorithmic approaches achieve an equivalent of *hardware demodulation* (above) by aliasing the bandpass signal into its passband via undersampling [29]–[31], [33]. This is schematically explained in Fig. 4 and the focus of our work.

—*Unlimited Sampling of Bandpass Signals.* The widespread prevalence of bandpass signals, also studied in the hardware context necessitates, the development of associated HDR ADCs (cf. [39]–[41]). Such

²We remind the reader that the transform domain separation principle in [4] is also applicable to aperiodic signals. The periodicity assumption leads to an efficient implementation via the Fast Fourier Transform (FFT) algorithm.

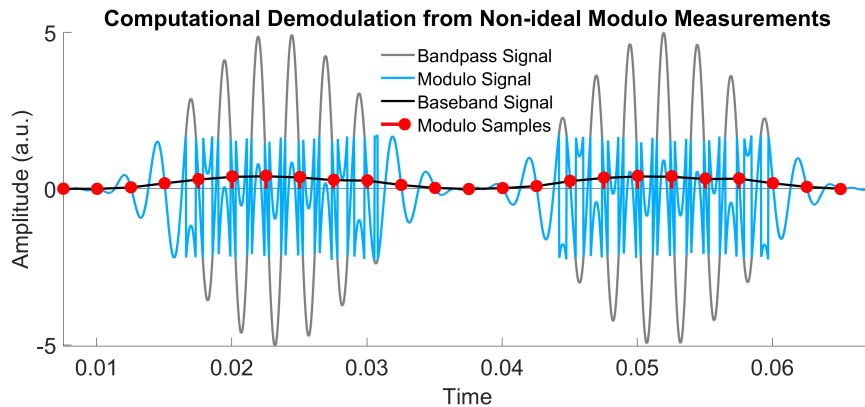


Fig. 2. An amplitude modulated signal, its associated modulo signal and undersampled modulo samples. The frequencies of the message and carrier signals are $f_M = 35$ Hz and $f_C = 400$ Hz, respectively. For a sampling period $T_S = 2.5$ ms, modulo samples coincide with underlying baseband signal samples, which directly results in demodulation.

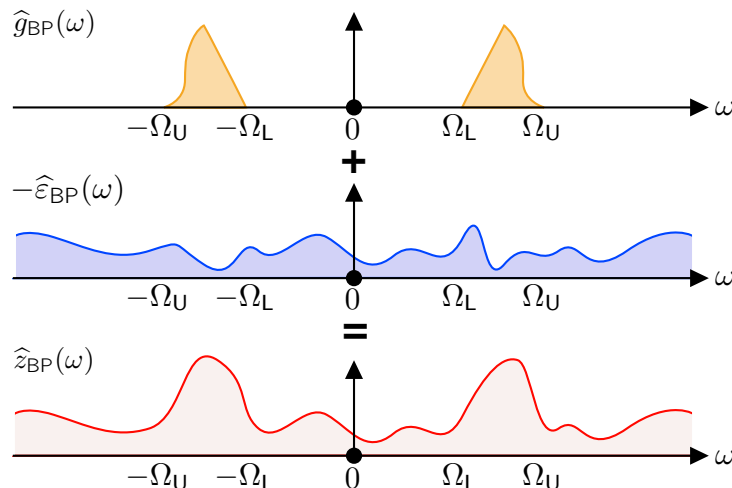


Fig. 3. The Fourier-domain representation of a modulo signal. The sum of a bandpass component $\hat{g}_{BP}(\omega)$ (upper) and a residual component $-\hat{\varepsilon}_{BP}(\omega)$ (middle) composes the modulo signal $\hat{z}_{BP}(\omega) = \hat{g}_{BP}(\omega) - \hat{\varepsilon}_{BP}(\omega)$ (lower).

approaches do not leverage the co-design approach *e.g.* USF. From the computational sensing perspective, bandpass signals have not yet been incorporated in USF, yet they are highly relevant in known and emerging applications such as USF based radar [42], [43].

On the one hand, modulo folding renders a bandlimited signal, non-bandlimited [1] so it is expected that undersampling in the spirit of [29]–[31], [34]–[37], is likely to be a theoretical dead-end. On the other hand, in our hardware experiments with \mathcal{M} -ADC and amplitude-modulated (AM) bandpass signals, we have observed something surprising; in certain settings, undersampling an AM signal with \mathcal{M} -ADC allows us to directly access its baseband version *without* any need for recovery algorithms. A hardware example with our \mathcal{M} -ADC depicting this scenario is shown in Fig. 2. The preservation of the bandpass spectral features in this undersampled scenario, even though the energy of the modulo signal is distributed over infinite frequency support as illustrated in Fig. 3, indicates that there may be a certain structured form of aliasing. This observation raises the following questions

- Q₁) Under what conditions one can recover a bandpass signal from undersampled, folded samples?
- Q₂) Can the undersampling strategy be applied to different signal folding architectures arising in

practice?

Q₃) Can the related recovery algorithms be validated using real experiments with the \mathcal{M} -ADC?

Contributions. In this work, we formulate and address the problem of HDR sampling and recovery of bandpass signals with modulo non-linearities, especially with an emphasis on undersampling. Our main contributions are as follows,

- 1) Given folded samples, we provide recovery guarantees for bandpass signals acquired at low sampling rates that enable sub-Nyquist sampling (see Fig. 1).
- 2) By considering different modulo folding architectures that explain hardware observations, namely, (a) ideal, (b) generalized modulo non-linearities, and (c) non-ideal architectures, our work offers algorithmic flexibility for practical solutions.
- 3) Beyond numerical simulations, we validate our theoretical results and algorithms via hardware experiments, thus closing the gap between theory and practice. This also establishes the empirical robustness of our recovery methods.

The far-reaching goal of our work is to enable HDR computational sampling of bandpass signals, which arise in a number of applications [32]–[38] including USF-Radar [42], [43]. Compared with the bandlimited signals, our recovery guarantees are summarized in Fig. 1.

II. SIGNAL FOLDING ARCHITECTURES

In this section, we revisit the ideal [1], [3], generalized [13] and non-ideal modulo operators [4], motivated from practical scenarios and hardware experiments. We also summarize the corresponding recovery algorithms that will be re-purposed to handle bandpass signals, thus increasing the applicability to a wider range of signal folding architectures.

A. Ideal Modulo Folding (\mathcal{M}_λ)

Acquisition. In the ideal case, folded samples are acquired using the centered modulo mapping defined by,

$$\mathcal{M}_\lambda : g \mapsto 2\lambda \left(\left\lfloor \frac{g}{2\lambda} + \frac{1}{2} \right\rfloor - \frac{1}{2} \right), \quad \llbracket g \rrbracket \stackrel{\text{def}}{=} g - \lfloor g \rfloor \quad (1)$$

where $\lfloor g \rfloor$ defines the floor function³. Even when $g \gg \lambda$, the range of \mathcal{M}_λ is bounded or $\mathcal{M}_\lambda(g(t)) \in [-\lambda, \lambda)$. For a sampling period $T_S > 0$, we denote modulo samples by $y[k] = \mathcal{M}_\lambda(g(kT_S))$ while $\gamma[k] = g(kT_S)$. A hardware prototype of the modulo ADC was presented in [4].

Reconstruction Strategy. From the modulo decomposition,

$$g(t) = \mathcal{M}_\lambda(g(t)) + \varepsilon_g(t), \quad \varepsilon_g \in 2\lambda\mathbb{Z} \quad (2)$$

we can deduce that unfolding $y[k]$ is equivalent to recovering $r[k] = \varepsilon_g(kT_S) \in 2\lambda\mathbb{Z}$ (residue) which is a simple function [3]. This recovery approach was first introduced in the Unlimited Sampling Algorithm or US-Alg [3]. Key to the recovery in US-Alg is the idea that $r[k]$ can be extracted from $y[k]$. For any $g \in \mathcal{B}_\Omega$,

³Greatest integer less than or equal to g i.e., $\lfloor g \rfloor = \max \{k \in \mathbb{Z} \mid k \leq g\}$.

its samples are highly correlated and hence, $\|\Delta^N \gamma\|_\infty \leq (T_S \Omega e)^N \|\gamma\|_\infty$. This implies that oversampling shrinks the higher order differences, $(\Delta^N \gamma)[k]$. Choosing,

$$T_S \leq T_{US} = \frac{1}{2\Omega e} \text{ and } N^* \geq \left\lceil \frac{\log \lambda - \log \beta_g}{\log (T_S \Omega e)} \right\rceil \quad (3)$$

with $\beta_g \geq \|g\|_\infty, \beta_g \in 2\lambda\mathbb{Z}$ it is guaranteed that $\|\Delta^{N^*} \gamma\|_\infty < \lambda$ [3]. For $\{T_S, N^*\}$ above, it follows that $\Delta^{N^*} \gamma = \mathcal{M}_\lambda(\Delta^{N^*} \gamma) = \mathcal{M}_\lambda(\Delta^{N^*} y)$ or $\Delta^{N^*} \varepsilon_g = \mathcal{M}_\lambda(\Delta^{N^*} y) - \Delta^{N^*} y$. Thereon, stable inversion of Δ^{N^*} is facilitated by leveraging the restriction on the residual function's amplitudes or $\varepsilon_g(kT) \in 2\lambda\mathbb{Z}$ and growth properties of $g \in \mathcal{B}_\Omega$. Finally, $g(t)$ is obtained by interpolating $\gamma[k] = y[k] + r[k]$.

B. Generalized Modulo Nonlinearity (\mathcal{M}_H)

A generalized modulo architecture or \mathcal{M}_H [13]–[17] was proposed to tackle fundamental hardware non-idealities *e.g.* *hysteresis* which is present during ADC quantization. This means that the threshold is different when the input signal is increasing or decreasing. Since modulo samples can be interpreted as *quantization noise* relative to the continuous input [27], it was argued that the hysteresis effect is also present in \mathcal{M}_λ -ADCs [14]. Including hysteresis in \mathcal{M}_H is beneficial to the model, allowing to tackle non-standard sampling scenarios such as incomplete folds [13], non-pointwise average sampling [15], or event-driven sampling [16], [17].

Acquisition. We define the \mathcal{M}_H as follows.

Definition 1 (Generalized Modulo). *The analog modulo encoder with threshold λ , hysteresis parameter $h \in [0, 2\lambda)$ and transient parameter α , is an operator $\mathcal{M}_H : L^2(\mathbb{R}) \rightarrow L^2(\mathbb{R})$, $\mathbf{H} = [\lambda, h, \alpha]$, that generates an analog function $z(t) = \mathcal{M}_H g(t)$, $t \geq \tau_0$ in response to input $g \in \text{PW}_\Omega$ defined by*

$$z(t) = g(t) - \varepsilon_H(t),$$

where

$$\varepsilon_H(t) = \sum_{p \in \mathbb{Z}} s_p \varepsilon_0(t - \tau_p), \quad t \in \mathbb{R}$$

is known as the residual,

$$\varepsilon_0(t) = 2\lambda_h \left[(1/\alpha) t \cdot \mathbb{1}_{[0, \alpha)}(t) + \mathbb{1}_{[\alpha, \infty)}(t) \right],$$

$\lambda_h = \lambda - h/2$, $s_p = \text{sign}(g(\tau_p) - g(\tau_{p-1}))$, $p \geq 1$ and $\{\tau_p\}$ is an asynchronous sequence satisfying $\tau_0 = 0$ and

$$\begin{aligned} \tau_1 &= \min \{t > \tau_0 \mid \mathcal{M}_\lambda(g(t) + \lambda) = 0\} \\ \tau_{p+1} &= \min \{t > \tau_p \mid \mathcal{M}_\lambda(g(t) - g(\tau_p) + h s_p) = 0\}. \end{aligned}$$

The \mathcal{M}_H operator was shown to accurately describe the experimentally observed output of the \mathcal{M} -ADC for different values of the design parameter h^4 .

⁴To get a sense of the hardware functionality, we refer the reader to the live hardware demonstration here: <https://youtu.be/R4rji5j0jD8>.

Reconstruction Strategy. The typical assumption is that the input belongs to $L^2(\mathbb{R}) \cap \mathcal{B}_\Omega$, also known as the Paley-Wiener space PW_Ω . We filter the data with ψ_N , which leads to

$$\psi_N * y[k] = \psi_N * \gamma[k] - \psi_N * r[k],$$

where $r[k] = \varepsilon_{\mathbf{H}}(kT)$ and ψ_N can be the finite difference filter Δ^N [13] or a generalized filter allowing additional noise robustness [14]. The general idea is to compute $r[k]$ and then $\gamma[k] = y[k] + r[k]$. Thus, the only unknowns are the folding times τ_p and signs s_p . Generally, when the transient duration α is not negligible, the recovery is performed via *thresholding*, exploiting that $\psi_N * r[k]$ consists of pulses centered in each folding time, with shape given by $\zeta_N[k] = \sum_{i=-\infty}^k \psi_N[i]$, the step response of ψ_N . Thresholding requires that $\psi_N * \gamma[k]$ is small and that the folding times are separated so that the pulses corresponding to different folds do not overlap. This can be enabled via the hysteresis parameter h allowing a lower bound on the spacing between folds $\tau_{p+1} - \tau_p \geq \frac{h}{\Omega \|g\|_\infty}$. For $\psi_N = \Delta^N$, the thresholding recovery conditions are [13]

- 1) $(T\Omega e)^N \|g\|_\infty + 2^N \eta_\infty \leq \frac{\lambda h}{2^N}$,
- 2) $(N+1)T\Omega \|g\|_\infty \leq h^*$, $h^* = \min\{h, 2\lambda - h\}$.

If α is negligible, then the recovery can also be performed with US-Alg, as will be detailed in Section III-B.

C. Non-Ideal Modulo Folding ($\widetilde{\mathcal{M}}_\lambda$)

In practice, despite its simplicity, ε_g satisfies $\varepsilon_g \notin 2\lambda\mathbb{Z}$. In that case, any algorithm that assumes $\varepsilon_g \in 2\lambda\mathbb{Z}$ will fail to recover the residue signal⁵. This required flexible algorithms that are agnostic to λ and can handle $\varepsilon_g \notin 2\lambda\mathbb{Z}$.

Acquisition. The non-ideal modulo operator $\widetilde{\mathcal{M}}_\lambda(\cdot)$ [4] is implicitly defined via $g(t) = \widetilde{\mathcal{M}}_\lambda(g(t)) + \mathcal{R}_g(t)$ where,

$$\mathcal{R}_g(t) = \sum_{m \in \mathcal{M}} c_m \mathbb{1}_{\mathcal{D}_m}(t), \quad \cup_m \mathbb{1}_{\mathcal{D}_m} = \mathbb{R}, \quad c_m \in \mathbb{R}. \quad (4)$$

\mathcal{M} is the set of folding instants, $\mathcal{D} \subseteq \mathbb{R}$ and unlike ε_g in (2), \mathcal{R}_g can take arbitrary real values. The non-ideal residue in (4) can describe (a) the effect of reset- or shot-noise disruptions on the sampled signal [10], (b) imperfections in the acquisition device [15] and, (c) deviations in the modulo threshold.

Reconstruction Strategy. To recover $g \in \mathcal{B}_\Omega$ from $y[k] = \widetilde{\mathcal{M}}_\lambda(g(kT_S))$, the ‘‘Fourier-Prony’’ algorithm or US-FP was devised in [4]. The US-FP seeks to recover $r[k] = \mathcal{R}_g[k]$ in the Fourier-domain while making no assumptions about λ . Instead, the spectral properties of $y[k]$ and the $g \in \mathcal{B}_\Omega$ are exploited to achieve a Fourier-domain separation between $\gamma[k]$ and $r[k]$ ⁶. It was shown that using the US-FP algorithm, a τ -periodic, Ω -bandlimited signal folded at most M times can be exactly recovered (up to a constant) from its modulo samples if the sampling period obeys,

$$T_S \leq T_{\text{FD}} = \frac{\tau}{K} \quad \text{where} \quad K \geq 2 \left(\left\lceil \frac{\Omega\tau}{2\pi} \right\rceil + M + 1 \right). \quad (5)$$

⁵In the example of the US-Alg, $g \in \mathcal{B}_\Omega$ and $\varepsilon_g \notin 2\lambda\mathbb{Z}$ can no longer be separated by Δ^N operation because $\varepsilon_g \notin 2\lambda\mathbb{Z} \Rightarrow \Delta^N \gamma \neq \mathcal{M}_\lambda(\Delta^N \gamma)$.

⁶Note that $g \in \mathcal{B}_\Omega$ but $\widetilde{\mathcal{M}}_\lambda(g(t)) \notin \mathcal{B}_\Omega$. The spectrum of $\widetilde{\mathcal{M}}_\lambda(g)$ can be split into an in-band component ($g \in \mathcal{B}_\Omega$) and an out-of-band component that only contains \mathcal{R}_g . Furthermore, the parametric structure of \mathcal{R}_g with the number of parameters depending on the folding instances, dictates the number of out-of-band accessible values that are required for the recovery of $r[k]$.

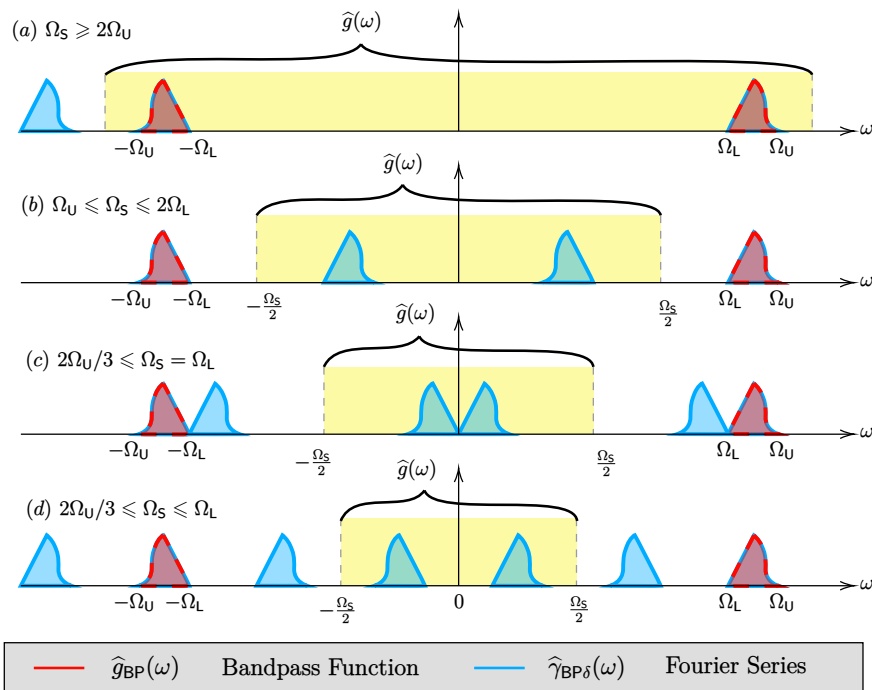


Fig. 4. The computation of the baseband function $g(t)$. The Fourier transform of the bandpass function (red), and periodicity of the Fourier series of the bandpass samples (blue) at four sampling frequencies. (a) Sampling above the critical rate of the bandpass signal. (b) Sampling frequency within the wedge of $P = 2$. (c) Maximal valid sampling frequency for $P = 3$. (d) Sampling frequency within the wedge of $P = 3$.

With T_S above, spectral estimation techniques are harnessed by US-FP to robustly recover $r[k]$ and hence $g(t)$.

III. TOWARDS COMPUTATIONAL DEMODULATION VIA MODULO UNDERSAMPLING

In the following, we consider a real-valued bandpass signal $g_{\text{BP}} \in \mathcal{B}_{(\Omega_L, \Omega_U)} \subseteq \mathcal{B}_{\Omega_U}$, where $0 < \Omega_L < \Omega_U$. We can use (2) to write $z_{\text{BP}}(t) = \mathcal{M}_\lambda(g_{\text{BP}}(t)) = g_{\text{BP}}(t) - \varepsilon_{g_{\text{BP}}}(t)$. The samples of $z_{\text{BP}}(t)$ at intervals of $T_S = 2\pi/\Omega_S$ are

$$y_{\text{BP}}[k] \stackrel{\text{def}}{=} z_{\text{BP}}(t)|_{t=kT_S} = \underbrace{g_{\text{BP}}(t)|_{t=kT_S}}_{=\gamma_{\text{BP}}[k]} - \underbrace{\varepsilon_{g_{\text{BP}}}(t)|_{t=kT_S}}_{=r_{\text{BP}}[k]}. \quad (6)$$

Since $g_{\text{BP}}(t) \in \mathcal{B}_{\Omega_U}$, we can reinterpret a bandpass signal as a bandlimited signal with bandwidth Ω_U and thus, the recovery methods of the USF apply. A naive reconstruction approach to obtain $g_{\text{BP}}(t)$ from modulo samples $y_{\text{BP}}[k]$ would entail working with the three recovery models in Section II and the corresponding sampling periods given in Fig. 1. Since this approach does not exploit $\widehat{g}_{\text{BP}}(\omega) = 0, \forall \omega \in [-\Omega_L, \Omega_L]$, we observe that the corresponding USF sampling periods are exorbitant, and often impractical in real-world scenarios.

This paper focuses on a *computational sensing* framework for efficient sampling of folded bandpass signals. Before we discuss the context of modulo samples, we discuss the conventional setup [29]–[31] and revisit the concept of *sampling-based-demodulation*. In this case, the natural interplay between the following two entities is leveraged,

- Fourier-domain bandpass structure.
- Spectral shifting by controlling sampling rate.

Sampling a signal at period T_S replicates its spectral content on intervals with period Ω_S . If Ω_S is smaller than the critical period of $2\Omega_U$, the replicas alias inside $(-\Omega_L, \Omega_L)$, and a corresponding lowpass signal can be extracted. We qualitatively demonstrate this for 4 exemplary periods in Fig. 4. When $\Omega_S \leq 2\Omega_U$, as in Fig. 4(b)-(d), the lowpass signal appears within the zero-centered band of $(-\Omega_L, \Omega_L)$. Notice the spectrum mirroring effect in Fig. 4(b). For recovery to be possible, the aliased replicas must not overlap. The conditions for non-overlapping spectral lobes are formalized in the next lemma, also known as the bandpass sampling theorem [30].

Lemma 1. *Let $g_{BP} \in \mathcal{B}_{(\Omega_L, \Omega_U)}$ be a continuous-time bandpass signal and let $\gamma_{BP}[k]$ be its uniform samples with $T_S \leq \pi/\Omega_{U,L}$ where $\Omega_{U,L} \stackrel{\text{def}}{=} \Omega_U - \Omega_L$. Define $\hat{\gamma}_{BP\delta}(\omega) = T_S \sum_{k \in \mathbb{Z}} \gamma_{BP}[k] e^{-j\omega k T_S}$. If there exists $P \in \mathbb{N}$ such that,*

$$\frac{\pi(P-1)}{\Omega_L} \leq T_S \leq \frac{\pi P}{\Omega_U}, \quad (7)$$

then $\hat{\gamma}_{BP\delta}(\omega) = \hat{g}_{BP}(\omega)$, $\omega \in (-\Omega_U, -\Omega_L) \cup (\Omega_L, \Omega_U)$ and $g_{BP}(t)$ can be recovered from $\gamma_{BP}[k]$.

In Lemma 1, P is a integer constant such that there are $P-1$ periods within $(-\Omega_L, \Omega_L)$, i.e., $\lfloor \frac{2\Omega_L}{\Omega_S} \rfloor = P-1 \in \mathbb{N}$. For Ω_S and P satisfying Lemma 1 and given $\gamma[k] \stackrel{\text{def}}{=} g(kT_S)$, we define $\hat{\gamma}_\delta(\omega) \stackrel{\text{def}}{=} T_S \sum_{k \in \mathbb{Z}} \gamma[k] e^{-j\omega k T_S}$. Then $g_{BP}(t)$ can be obtained by computing the inverse FT of,

$$\hat{g}_{BP}(\omega) = \mathbb{1}_{\mathcal{D}(\Omega_S, P)}(\omega) \hat{\gamma}_\delta(\omega), \quad \text{where} \quad (8)$$

$$\mathcal{D}(\Omega_S, P) = \frac{1}{2}[-P\Omega_S, -(P-1)\Omega_S] \cup \frac{1}{2}[(P-1)\Omega_S, P\Omega_S].$$

From Spectral Overlap to Bandpass Recovery. Sampling-based-demodulation is designed so that bandpass content occupies the vacant lowpass regions via aliasing. Adapting this strategy to the USF is highly non-trivial as $z_{BP}(t) \notin \mathcal{B}_{(\Omega_L, \Omega_U)}$. The relation between the bandpass and the residual components is shown in Fig. 3, and reveals that for modulo bandpass signals there is no interval on which $\hat{z}_{BP}(\omega) = \hat{g}_{BP}(\omega) - \hat{\varepsilon}_{g_{BP}}(\omega) = 0$. Therefore, previous approaches do not apply [29]–[31]. Nonetheless, the example in Fig. 2 implies that spectral overlapping does not necessarily prevent demodulation, albeit in the context of bandpass signals. On the flip side, we show that one can demodulate even non-bandpass signals such as $\hat{z}_{BP}(\omega)$ by sampling. The goal of this paper is to develop mathematical guarantees and frameworks for computational demodulation of modulo signals. By looking at the two components of a modulo signal (2), the task is to determine the intersection between sampling periods that,

- 1) do not create spectral overlap of $g_{BP}(t)$, and,
- 2) are sufficient to recover the residual samples.

A. Undersampling with the Ideal Modulo Architecture

In what follows, we prove a sampling theorem enabling ideal modulo sampling of bandpass signals with a sampling rate that improves the known result $T_S \leq T_{US} = 1/2\Omega_e$ (3).

Theorem 1 (The Unlimited Bandpass Sampling Theorem). *Let $g_{BP}(t) \in \mathcal{B}_{(\Omega_L, \Omega_U)}$ and $z_{BP}(t) = \mathcal{M}_\lambda(g_{BP}(t))$. Let $y_{BP}[k] = z(kT_S)$, $k \in \mathbb{Z}$ be the modulo samples of $g_{BP}(t)$ at period $T_S > 0$. If there exists $P \in \mathbb{N}$ such that T_S satisfies,*

$$\begin{cases} \frac{\pi(P-1)}{\Omega_L} \leq T_S \leq \frac{2\pi e(P-1)+1}{2e\Omega_U} & P \in 2\mathbb{N} + 1 \\ \frac{2\pi e P - 1}{2e\Omega_L} \leq T_S \leq \frac{\pi P}{\Omega_U} & P \in 2\mathbb{N} \end{cases} \quad (9)$$

where e denotes Euler's number, then $g_{\text{BP}}(t)$ can be recovered from $y_{\text{BP}}[k]$ up to an integer multiple of 2λ .

Proof. We define the normalized FS with coefficients $y_{\text{BP}}[k]$,

$$\begin{aligned} \widehat{y}_{\text{BP}\delta}(\omega) &\stackrel{\text{def}}{=} T_{\text{S}} \sum_{k \in \mathbb{Z}} y_{\text{BP}}[k] e^{-j\omega k T_{\text{S}}} \\ &\stackrel{(6)}{=} T_{\text{S}} \sum_{k \in \mathbb{Z}} [\gamma_{\text{BP}} - r_{\text{BP}}][k] e^{-j\omega k T_{\text{S}}} = [\widehat{\gamma}_{\text{BP}\delta} - \widehat{r}_{\text{BP}\delta}](\omega), \end{aligned} \quad (10)$$

and the lowpass filtered signal $g(t)$ via its spectrum,

$$\widehat{g}(\omega) = \mathbb{1}_{\left[-\frac{\Omega_{\text{S}}}{2}, \frac{\Omega_{\text{S}}}{2}\right]}(\omega) \widehat{\gamma}_{\text{BP}\delta}(\omega). \quad (11)$$

Using that $T_{\text{S}}\gamma_{\text{BP}}[k]$ are the FS coefficients of $\widehat{\gamma}_{\text{BP}\delta}(\omega)$ together with (11) we write,

$$\begin{aligned} \gamma_{\text{BP}}[k] &= \frac{1}{2\pi} \int_{-\Omega_{\text{S}}/2}^{\Omega_{\text{S}}/2} \widehat{\gamma}_{\text{BP}\delta}(\omega) e^{j\omega k T_{\text{S}}} d\omega \\ &= \frac{1}{2\pi} \int_{-\infty}^{\infty} \mathbb{1}_{\left[-\frac{\Omega_{\text{S}}}{2}, \frac{\Omega_{\text{S}}}{2}\right]}(\omega) \widehat{\gamma}_{\text{BP}\delta}(\omega) e^{j\omega k T_{\text{S}}} d\omega \\ &\stackrel{(11)}{=} \frac{1}{2\pi} \int_{-\infty}^{\infty} \widehat{g}(\omega) e^{j\omega k T_{\text{S}}} d\omega = g(t)|_{t=kT_{\text{S}}} \stackrel{\text{def}}{=} \gamma[k]. \end{aligned} \quad (12)$$

We can use (2) to write $g(t) = z(t) + \varepsilon_g(t)$, where $z(t) = \mathcal{M}_{\lambda}(g(t))$. Respectively, we write the samples $\gamma[k]$ as,

$$\gamma[k] = y[k] + r[k]. \quad (13)$$

The difference between the two discrete modulo sequences is,

$$y_{\text{BP}}[k] - y[k] = \underbrace{\gamma_{\text{BP}}[k] - \gamma[k]}_{=0 \text{ from (12)}} + r[k] - r_{\text{BP}}[k]. \quad (14)$$

For the LHS of (14), since $y_{\text{BP}}[k] \in [-\lambda, \lambda)$ and $-y_{\text{BP}}[k] \in (-\lambda, \lambda]$, we get that $y_{\text{BP}}[k] - y[k] \in (-2\lambda, 2\lambda)$. For the RHS, $r[k] - r_{\text{BP}}[k] \in 2\lambda\mathbb{Z}$. Hence, the intersection set between the two sides of (14) must be zero and we get,

$$y_{\text{BP}}[k] - y[k] = r[k] - r_{\text{BP}}[k] = 0 \Rightarrow y_{\text{BP}}[k] = y[k]. \quad (15)$$

Substituting (12) and (15) into (10) we get,

$$\widehat{y}_{\text{BP}\delta}(\omega) = \widehat{y}_{\delta}(\omega) = \widehat{\gamma}_{\delta}(\omega) - \widehat{r}_{\delta}(\omega), \quad (16)$$

where $\widehat{\gamma}_{\delta}(\omega)$ and $\widehat{r}_{\delta}(\omega)$ are the FS of $\gamma[k]$ and $r[k]$, respectively. From (16), we get that $\widehat{y}_{\delta}(\omega) = \widehat{\gamma}_{\delta}(\omega) - \widehat{r}_{\delta}(\omega)$ which means that under the conditions of the US theorem [3] we can get $\gamma[k]$ (and hence, $g(t)$) from $y_{\text{BP}}[k]$. Moreover, if (7) is satisfied then from Lemma 1, $g_{\text{BP}}(t)$ can be obtained and

$$\Omega_{\text{U}}^g = \begin{cases} \Omega_{\text{U}} - \frac{P-1}{2}\Omega_{\text{S}} & P \in 2\mathbb{N} + 1 \\ \frac{P}{2}\Omega_{\text{S}} - \Omega_{\text{L}} & P \in 2\mathbb{N} \end{cases}, \quad (17)$$

where Ω_{U}^g is the bandwidth of g . The USF recovery condition for $g(t)$ requires that $\Omega_{\text{S}} \geq 4\pi\Omega_{\text{U}}^g e$. For

$P \in 2\mathbb{N} + 1$, plugging (17) allows to re-write the USF recovery condition as

$$\begin{aligned} \Omega_S &\geq 4\pi\Omega_U^g e = 4\pi e \left(\Omega_U - \frac{P-1}{2}\Omega_S \right) \\ &\Leftrightarrow \Omega_S \geq \frac{4\pi e}{1+2\pi e(P-1)}\Omega_U. \end{aligned} \quad (18)$$

It can be directly shown that $\frac{4\pi e}{1+2\pi e(P-1)}\Omega_U \geq \frac{2\Omega_U}{P}$, which yields the final condition on Ω_S ,

$$\frac{4\pi e}{1+2\pi e(P-1)}\Omega_U \leq \Omega_S \leq \frac{2\Omega_L}{P-1}. \quad (19)$$

For $P \in 2\mathbb{N}$, using the same derivation as in (18), we get $\Omega_S \geq 4\pi e \left(\frac{P}{2}\Omega_S - \Omega_L \right)$, which yields

$$\frac{2\Omega_U}{P} \leq \Omega_S \leq \frac{4\pi e}{2\pi e P - 1}\Omega_L. \quad (20)$$

Using $T_S = \frac{2\pi}{\Omega_S}$ in (19,20) yields the desired result; then $g_{\text{BP}}(t)$ can be recovered from its modulo samples.

■

Theorem 1 is consistent with (3). Given that $g_{\text{BP}} \in \mathcal{B}_{[\Omega_L, \Omega_U]} \subseteq \mathcal{B}_{\Omega_U}$, if we sample above the critical rate we have $P = 1$ and thus condition (19) is satisfied for $T_S \leq T_{U_S}$. Nevertheless, for $P > 1$, the bandpass prior is exploited and this results in lower sampling periods. In the bandpass result of [30], P is bounded by $P \leq \left\lfloor \frac{\Omega_U}{\Omega_{U,L}} \right\rfloor$. We can find an equivalent bound for the modulo bandpass case from (19) and (20) as,

$$\begin{cases} (P-1)2\pi e\Omega_{U,L} \leq \Omega_L & P \in 2\mathbb{N} + 1 \\ 2\pi e P \Omega_{U,L} \leq \Omega_U & P \in 2\mathbb{N} \end{cases}$$

which implies that,

$$\begin{cases} P \leq \left\lfloor \frac{\Omega_L}{2\pi e\Omega_{U,L}} + 1 \right\rfloor & P \in 2\mathbb{N} + 1 \\ P \leq \left\lfloor \frac{\Omega_U}{2\pi e\Omega_{U,L}} \right\rfloor & P \in 2\mathbb{N} \end{cases}. \quad (21)$$

Since the bound in (21) is tighter for the even case, we get that $P \leq \left\lfloor \frac{\Omega_U}{2\pi e\Omega_{U,L}} \right\rfloor$, which is stricter than $P \leq \left\lfloor \frac{\Omega_U}{\Omega_{U,L}} \right\rfloor$. The sampling frequencies from Theorem 1 that achieve minimal bandwidth $\Omega_U^g = \Omega_{U,L}$ for g are

$$\begin{cases} \Omega_S = \frac{2}{P-1}\Omega_L & P \in 2\mathbb{N} + 1 \\ \Omega_S = \frac{2}{P}\Omega_U & P \in 2\mathbb{N} \end{cases} \quad (22)$$

which produce the *baseband relocation* cases, and demonstrated in Fig. 4(c) for $P = 3$.

Sampling-Based Demodulation of Modulo AM Signals. There are particular cases where the result of Theorem 1 can be improved based on an even stronger prior. For example, we can consider the case of double-sideband AM signals [44], which are bandpass functions whose spectrum is consisted of two adjacent sidebands that are mirrored around a carrier frequency. These signals are among the most common waveforms that are encountered in practical applications. Because of their spectral structure, AM signals can be recovered even when $\Omega_S = \Omega_{U,L}$ [29]. In the next corollary, we extend this result for modulo-folded AM signals.

Corollary 1 (Unlimited Sampling of AM Signals). *If the side lobes of \hat{g} are symmetric, i.e., $\hat{g}(\Omega_L + \omega) =$*

Algorithm 1: Bandpass Recovery via Unlimited Sensing

Input: $y_{\text{BP}}[k]$, $\lambda, \beta_{g_{\text{BP}}} = \|g_{\text{BP}}\|_{\infty}$, Ω_{L} , and Ω_{U} .

Result: Bandpass function, $\tilde{g}_{\text{BP}}(t)$.

- 1) Compute Ω_{U}^g using (17).
 - 2) Compute $N = \left\lceil \frac{\log \lambda - \log \beta_{g_{\text{BP}}}}{\log(T_s \Omega_{\text{U}}^g e)} \right\rceil$.
 - 3) Compute $(\Delta^N y)[k] \stackrel{(15)}{=} (\Delta^N y_{\text{BP}})[k]$.
 - 4) Compute $(\Delta^N r)[k] = (\mathcal{M}_{\lambda}(\Delta^N y) - (\Delta^N y))[k]$.
Set $s_{(0)}[k] = (\Delta^N r)[k]$.
 - 5) For $n = 0 : N - 2$
 - (i) $s_{(n+1)}[k] = \mathbf{S}(s_{(n)})[k]$, $\mathbf{S} : \{s[k]\}_{k \in \mathbb{Z}^+} \rightarrow \sum_{m=1}^k s[m]$.
 - (ii) $s_{(n+1)}[k] = 2\lambda \left\lfloor \frac{\lfloor s_{(n+1)}/\lambda \rfloor}{2} \right\rfloor$ (rounding to $2\lambda\mathbb{Z}$).
 - (iii) Compute $\kappa_{(n)} = \left\lfloor \frac{\mathbf{S}^2(\Delta^n r)[1] - \mathbf{S}^2(\Delta^n r)\left[\frac{6\beta_{g_{\text{BP}}}}{\lambda} + 1\right]}{12\beta_{g_{\text{BP}}}} + \frac{1}{2} \right\rfloor$.
 - (iv) $s_{(n+1)}[k] = s_{(n+1)}[k] + 2\kappa_{(n)}$.

end
 - 6) $\tilde{\gamma}[k] = \mathbf{S}(s_{(N-1)})[k] + y_{\text{BP}}[k] + 2m\lambda$, $m \in \mathbb{Z}$.
 - 7) Compute $\hat{\gamma}_{\delta}(\omega) = T_s \sum_{k \in \mathbb{Z}} \tilde{\gamma}[k] e^{-j\omega k T_s}$.
 - 8) Estimate $\tilde{g}_{\text{BP}}(t)$ from $\hat{\gamma}_{\delta}(\omega)$ using (8) and P from (9).
-

$\hat{g}(\Omega_{\text{U}} - \omega)$, $\forall \omega \in [0, \Omega_{\text{U,L}}/2]$, then $g_{\text{BP}}(t)$ can be recovered via Algorithm 1 if there exists $P_{\text{AM}} \in \mathbb{N}$ such that

$$\Omega_{\text{S}} = \frac{\Omega_{\text{U}} + \Omega_{\text{L}}}{2P_{\text{AM}}} \quad \text{and} \quad \frac{\Omega_{\text{U}} + \Omega_{\text{L}}}{\Omega_{\text{U}} - \Omega_{\text{L}}} \geq 4\pi e P_{\text{AM}}. \quad (23)$$

Proof. We require that the sideband copies lead to pairs of lobes that perfectly overlap, such that a pair is centered around the origin. This is true if the LHS equation in (23) is satisfied. Furthermore, to ensure that adjacent pairs of lobes do not lead to additional overlaps, which ensures that the information can be recovered, we further assume $\Omega_{\text{S}} \geq \Omega_{\text{U,L}}$. This leads to the following condition on $\Omega_{\text{U}}, \Omega_{\text{L}}$:

$$\frac{\Omega_{\text{U}} + \Omega_{\text{L}}}{\Omega_{\text{U}} - \Omega_{\text{L}}} \geq 2P_{\text{AM}}. \quad (24)$$

Lastly, we compute Ω_{U}^g , in order to derive a bound for USF. The pair of lobes centered in the origin has width $\Omega_{\text{U}} - \Omega_{\text{L}}$, therefore its bandwidth is $\Omega_{\text{U}}^g = \frac{\Omega_{\text{U,L}}}{2}$. This yields the USF condition $\Omega_{\text{S}} \geq 4\pi e \frac{\Omega_{\text{U,L}}}{2} = 2\pi e \Omega_{\text{U,L}}$. By using the LHS equation in (23) it is translated in terms of $\Omega_{\text{U}}, \Omega_{\text{L}}$ that leads to the RHS equation in (23). ■

We remark that the RHS equation in (23) is a tighter condition than (24), and thus is enough for input recovery in the case of AM signals. As a particular case, we highlight the implication of Corollary 2 for sinusoids, which can be viewed as AM signals with a constant modulated amplitude, Q_{L} that corresponds to the carrier frequency and $\Omega_{\text{U,L}} \rightarrow 0$. While [9] demonstrated that these signals allow lower sampling rates than in the general bandlimited case, under the conditions of Corollary 2, this improvement can be further enhanced.

B. Undersampling with Generalized Modulo Architecture

Here, we assume that $g_{\text{BP}} \in \text{PW}_{[\Omega_L, \Omega_U]}$ is sampled with \mathcal{M}_{H} and $T_S > 0$. The goal is to recover $g_{\text{BP}}(kT_S)$ up to an integer multiple of λ_h . The output samples satisfy

$$y_{\text{BP}}[k] = \mathcal{M}_{\text{H}} g_{\text{BP}}(kT_S) = (\gamma_{\text{BP}} + r_{\text{BP}})[k] \stackrel{(12)}{=} (\gamma + r_{\text{BP}})[k], \quad (25)$$

where $g(kT_S)$ is defined in (11) and the residue $r_{\text{BP}}[k] = \sum_{p \in \mathbb{Z}} s_p \varepsilon_0(kT_S - \tau_p)$. We assume that the transient is negligible ($\alpha = 0$), and thus $\varepsilon_0(kT_S - \tau_p) = 2\lambda_h \mathbb{1}_{[\tau_p, \infty)}(kT_S) \in \{0, 2\lambda_h\}$. Therefore, samples $\gamma[k]$ (25) can be recovered up to $2\lambda_h \mathbb{Z}$ using a variation of US-Alg, as explained next. Using the same reasoning as in US-Alg, $\forall k \in \mathbb{Z}$ we require that $|\Delta^N (\gamma + \eta)[k]| < \lambda_h$, which is true if $(T_S \Omega e)^N \|g\|_{\infty} < \lambda_h$. Subsequently, $\tilde{\gamma}[k] = \gamma[k] + 2M\lambda_h, M \in \mathbb{Z}$, is computed using $\Delta^N \gamma[k] = \mathcal{M}_{\lambda_h}(\Delta^N y[k])$. In the following, we give a theorem guaranteeing recovery from generalized modulo data.

Theorem 2 (Generalized Modulo Recovery). *Let $g_{\text{BP}} \in \text{PW}_{[\Omega_L, \Omega_U]}$ and $y_{\text{BP}}[k] = \mathcal{M}_{\text{H}} g_{\text{BP}}(kT_S)$ be the generalized modulo samples of g_{BP} with sampling period $T_S > 0$. We assume that there exists $P \in \mathbb{N}$ such that T_S satisfies (9). Then g_{BP} can be recovered from $\Delta^N y_{\text{BP}}[k]$ up to an integer multiple of $2\lambda_h$, where N is defined as*

$$N = \left\lceil \frac{\log \lambda_h - \log \beta_g}{\log (T_S \Omega_U^g e)} \right\rceil, \quad (26)$$

and Ω_U^g is defined in (17).

Proof. From (25) we get that $\Delta^N y_{\text{BP}} = \Delta^N (\gamma + r_{\text{BP}})$, where $\gamma[k] = g(kT_S)$ and g is defined in (11). It can be directly verified that the value of N in (26) guarantees $(T_S \Omega e)^N \|g\|_{\infty} < \lambda_h$, which was also shown in [3] for the case $h = 0$. Similarly, given that $r_{\text{BP}}[k] \in \{2m\lambda_h \mid m \in \mathbb{Z}\}$, it can be directly shown that $\Delta^N r_{\text{BP}}[k] \in \{2m\lambda_h \mid m \in \mathbb{Z}\}$. Then, using a similar reasoning as for US-Alg, we get that $\mathcal{M}_{\lambda_h}(\Delta^N r_{\text{BP}}[k]) = 0$ and thus $\Delta^N \gamma[k] = \mathcal{M}_{\lambda_h}(\Delta^N y_{\text{BP}}[k])$. Further on, the US-Alg can be used to recover $g(t)$. Even though the recovery of $g(t)$ has no direct link to the bandpass property of $g_{\text{BP}}(t)$, this is required in order to get back $g_{\text{BP}}(t)$ from $g(t)$. As shown in Theorem 1, this is possible if (9) is satisfied. ■

C. Fourier-Domain Approach for Modulo Undersampling

The recovery procedure from non-ideal modulo samples exploits both the parametric structure of the residual signal (4), and the partitioning of the modulo signal in the frequency domain. For bandpass signals, two partitioning intervals can be leveraged for the signal recovery, since $\hat{g}_{\text{BP}}(\omega) = 0, \forall \omega \in \mathbb{R}, |\omega| \notin (\Omega_L, \Omega_U)$. As a first observation, we note that the bandpass prior interval of $\omega \in (-\Omega_L, \Omega_L)$ can be used to recover the residual signal's parameters without the need for demodulation, for any $\Omega_S > 2\Omega_U$. Qualitatively, this can be observed in Fig. 3. However, for further reduction of the sampling frequency, demodulation will be necessary.

Fourier-Domain Partitioning of Modulo Bandpass Signals. We use the DFT to develop the modulo bandpass sampling conditions in the discrete frequency domain. The function $g_{\text{BP}}(t)$ is considered to be τ -periodic. To avoid spectral leakage, we assume that $T_S = \frac{\tau}{K}$, where $K \in \mathbb{Z}$ denotes the number of

samples. Moreover, without reducing the generality, we assume that Ω_L, Ω_U are integer multiples of $\frac{2\pi}{\tau}$. Then we define $Q_L \in \mathbb{Z}$ and $Q_U \in \mathbb{Z}$ as

$$Q_L \stackrel{\text{def}}{=} \frac{K\Omega_L}{\Omega_S}, \quad Q_U \stackrel{\text{def}}{=} \frac{K\Omega_U}{\Omega_S}, \quad (27)$$

For $T_S > 0$, sampling $y_{\text{BP}}(t)$ over a period produces $K = \tau/T_S$ discrete samples. In terms of the K -length DFT of $y_{\text{BP}}[k]$, (16) becomes,

$$\begin{aligned} \widehat{y}_{\text{BP}}[n] &= T_S \sum_{k=0}^{K-1} y_{\text{BP}}[k] e^{-j\frac{2\pi}{K}kn} = \widehat{y}_{\text{BP}\delta}(\omega) \Big|_{\omega=\frac{2\pi}{\tau}n} \\ &= (\widehat{\gamma}_\delta - \widehat{r}_{\text{BP}\delta})(\omega) \Big|_{\omega=\frac{2\pi}{\tau}n} \\ &= \widehat{g}[n] - \widehat{r}_{\text{BP}}[n]. \end{aligned}$$

Moreover, $g(t)$ defined in (11) is τ -periodic as well, given that its frequencies are obtained by shifting $\widehat{g}_{\text{BP}}(\omega)$ by integer multiples of $\Omega_S = \frac{2\pi}{T_S}$.

Given that we assume $\Omega_L > 0$, we get $\Omega_L \geq 2\pi/\tau$ and thus $Q_L \geq 1$. We know that the values of the DFT of $\gamma[k] = g(kT_S)$ map to the magnitudes of $\widehat{g}(\omega) \Big|_{\omega=n\frac{2\pi}{\tau}=n\frac{\Omega_S}{K}}$. It then follows from (17) and (27) that the indices of the passband frequencies in $\widehat{g}[n]$, the DFT of $g(t)$, are contained in

$$\{-Q_U^g, Q_U^g + 1, \dots, -Q_L^g\} \cup \{Q_L^g, Q_L^g + 1, \dots, Q_U^g\},$$

where

$$Q_U^g = \begin{cases} Q_U - \frac{P-1}{2}K & P \in 2\mathbb{N} + 1 \\ \frac{P}{2}K - Q_L & P \in 2\mathbb{N} \end{cases} \quad \text{and}, \quad (28)$$

$$Q_L^g = Q_U^g - Q_{U,L},$$

where $Q_{U,L} \stackrel{\text{def}}{=} Q_U - Q_L$ and $P - 1 = \frac{2\Omega_L}{\Omega_S} \in \mathbb{N}$ represents the number of periods Ω_S within $(-\Omega_L, \Omega_L)$. We have that $g(kT_S) = g_{\text{BP}}(kT_S)$ via (12). Then, using the periodicity of the DFT $\widehat{y}_{\text{BP}}[K - q] = \widehat{y}_{\text{BP}}[q]$, $\forall q \in \{0, 1, \dots, K\}$, the following holds

$$\widehat{y}_{\text{BP}}[n] = \begin{cases} \widehat{g}[n] - \widehat{r}_{\text{BP}}[n], & n \in \mathbb{E}_{[Q_L^g, Q_U^g], K} \\ -\widehat{r}_{\text{BP}}[n], & n \in \mathbb{I}_K \setminus \mathbb{E}_{[Q_L^g, Q_U^g], K} \end{cases}$$

where the set $\mathbb{E}_{[Q_L^g, Q_U^g], K}$ is given by,

$$\mathbb{E}_{[Q_L^g, Q_U^g], K} = [Q_L^g, Q_U^g] \cup [K - Q_U^g, K - Q_L^g].$$

The partition is schematically illustrated in Fig. 5. As can be seen, the two sets on which the residual and the lowpass signals can be separated are,

$$\mathbb{F}_{\text{BP}} = \begin{cases} [Q_U^g + 1, K - Q_U^g - 1] & \text{(Outer Set)} \\ [0, Q_L^g - 1] \cup [K - Q_L^g - 1, K - 1] & \text{(Inner Set)} \end{cases}. \quad (29)$$

A sampling density criterion that enables recovery based on the two sets is given in the next theorem.

Theorem 3 (Bandpass Fourier-Domain Recovery). *Let $g_{\text{BP}} \in \mathcal{B}_{(\Omega_L, \Omega_U)}$ be a τ -periodic function. Suppose*

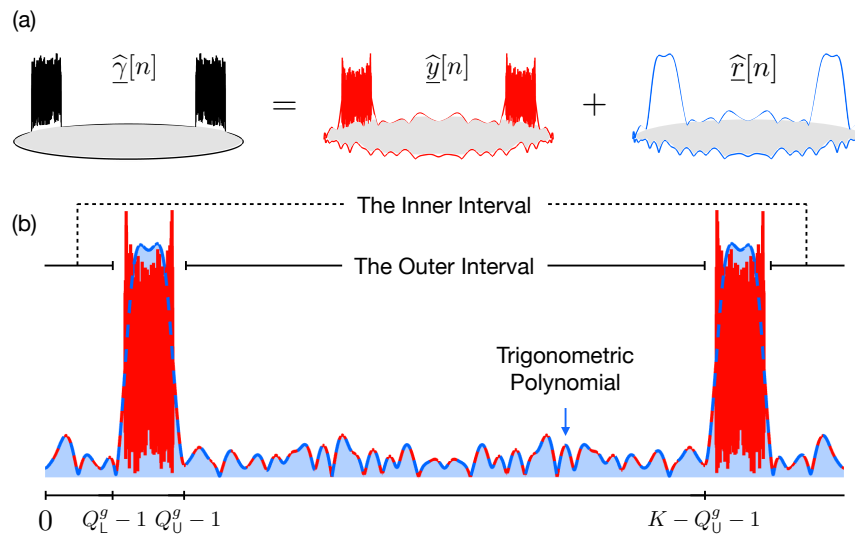


Fig. 5. The partitioning of a bandpass signal into its modulo (red) and residual (blue) components in the discrete Fourier domain. (a) Decomposition of the bandpass spectra into modulo and residual components. (b) The inner and outer intervals as defined in (29) on a single DFT period.

that we are given K modulo samples of $y_{\text{BP}}[k] = \widetilde{\mathcal{M}}_\lambda(g_{\text{BP}}(kT_S))$, at sampling period $T_S = \frac{\tau}{K} > 0$, folded at most M times. If there exists $P \in \mathbb{N}$ such that T_S satisfies,

$$\begin{cases} \frac{(P-1)\tau}{2Q_L} \leq T_S \leq \frac{P\tau}{2(Q_U+M+1)}, & P \in 2\mathbb{N} + 1 \\ \frac{(P-1)\tau}{2(Q_L-M-1)} \leq T_S \leq \frac{P\tau}{2Q_U}, & P \in 2\mathbb{N} \end{cases}$$

or,

$$\begin{cases} \frac{(P-1)\tau}{2(Q_L-M-1)} \leq T_S \leq \frac{P\tau}{2Q_U}, & P \in 2\mathbb{N} + 1 \\ \frac{(P-1)\tau}{2Q_L} \leq T_S \leq \frac{P\tau}{2(Q_U+M+1)}, & P \in 2\mathbb{N} \end{cases}, \quad (30)$$

and $Q_L > M + 1$ for $P \in 2\mathbb{N}$ or $P \in (2\mathbb{N} + 1) \setminus \{1\}$ in (30). Then, $g_{\text{BP}}(t)$ can be recovered from $y_{\text{BP}}[k]$ up to $2\lambda\mathbb{Z}$.

Proof. We start from (7) and multiply by K to get,

$$\left(\frac{P-1}{2}\right)K \leq \frac{K\Omega_L}{\Omega_S} \leq \frac{K\Omega_U}{\Omega_S} \leq \left(\frac{P}{2}\right)K. \quad (31)$$

Re-arranging (31) with respect to the number of samples K ,

$$\frac{2}{P} \frac{K\Omega_U}{\Omega_S} \leq K \leq \frac{2}{P-1} \frac{K\Omega_L}{\Omega_S}. \quad (32)$$

Then, using (27), we get an equivalent of the bandpass sampling condition (7) in the discrete frequency domain

$$\frac{2Q_U}{P} \leq K \leq \frac{2Q_L}{P-1}. \quad (33)$$

Next, to recover the bandpass samples we note that for a modulo sequence with M folds, the first order difference of the residual, $\underline{r}[k]$, is a $2M$ -parametric signal. Its recovery requires $2M + 1$ samples in the outer set (29), for which $\hat{y}_{\text{BP}}[n] = -\hat{r}_{\text{BP}}[n]$. This is guaranteed by $K - 2Q_U^g - 1 \geq 2M + 1$. By substituting

Algorithm 2: Bandpass Recovery in the Fourier-Domain

Input: $\{y_{\text{BP}}[k]\}_{k=0}^{K-1}$, τ , Ω_{L} , Ω_{U} , and $M = |\mathcal{M}|$ (4)

Result: Bandpass function, $\tilde{g}_{\text{BP}}(t)$.

- 1) Compute $\hat{y}_{\text{BP}}[n]$, the DFT of $y_{\text{BP}}[k]$.
 - 2) Compute Q_{U}^g or Q_{L}^g using (28).
 - 3) Define $\hat{r}[n] \stackrel{\text{def}}{=} -\hat{y}_{\text{BP}}[n] \stackrel{(15)}{=} -\hat{y}[n]$, where $n \in \mathbb{F}_{\text{BP}}$ (29).
 - 4) Use spectral estimation to estimate $\tilde{r}[k]$ [4].
 - 5) Estimate $\tilde{r}[k] = \sum_{m=1}^k \tilde{r}[m]$ (up to an unknown constant), and compute $\tilde{\gamma}[k] = \tilde{r}[k] + y_{\text{BP}}[k]$.
 - 6) Compute $\hat{\gamma}_{\delta}(\omega) = T_{\text{S}} \sum_{k \in \mathbb{Z}} \tilde{\gamma}[k] e^{-j\omega k T_{\text{S}}}$.
 - 7) Estimate $\tilde{g}_{\text{BP}}(t)$ from $\hat{\gamma}_{\delta}(\omega)$ using (8) and P from (30).
-

with Q_{U}^g from (28) and isolating K we get,

$$\begin{cases} K \geq \frac{2(Q_{\text{U}}+M+1)}{P} & P \in 2\mathbb{N} + 1 \\ K \leq \frac{2(Q_{\text{L}}-M-1)}{P-1} & P \in 2\mathbb{N} \end{cases}.$$

For every $M \geq 0, P > 0$, we get that,

$$\frac{2(Q_{\text{U}} + M + 1)}{P} \geq \frac{2Q_{\text{U}}}{P} \quad \text{and} \quad \frac{2(Q_{\text{L}} - M - 1)}{P - 1} \leq \frac{2Q_{\text{L}}}{P - 1}.$$

Integration with the bound in (33) and substitution $K = \tau/T_{\text{S}}$ yields the first condition in (30). For the set

$$[0, Q_{\text{L}}^g - 1] \cup [K - Q_{\text{L}}^g - 2, K - 2]$$

we require that $2(Q_{\text{L}}^g - 1) \geq 2M$. We use Q_{L}^g from (28) and isolate K to get,

$$\begin{cases} K \leq \frac{2(Q_{\text{L}}-M-1)}{P-1} & P \in 2\mathbb{N} + 1 \\ K \geq \frac{2(Q_{\text{U}}+M+1)}{P} & P \in 2\mathbb{N} \end{cases}. \quad (34)$$

As in the outer set case, we integrate (34) with the bound in (33), and replace $K = \tau/T_{\text{S}}$ to get the sampling condition in (30). For T_{S} that satisfies (30) for some $P \in \mathbb{N}$, $g_{\text{BP}}(t)$ can be recovered from its modulo samples by Algorithm 2. ■

Remarks on Theorem 3:

- For $Q_{\text{U}} = Q_{\text{U,L}}$ (bandlimited signal case), we return to the expected result that $2(M+1)$ modulo samples beyond the maximal non-zero frequency of the signal are needed.
- For $P = 1$, reconstruction from the inner set samples requires $Q_{\text{L}} \geq M + 1$, regardless of the sampling period.
- As P gets larger, more replicas of the bandwidth occupy the outer set (even P case) or the inner set (odd P case). Consequentially, fewer folds can be recovered.
- For a given P , the outer set (even P case) or the inner set (odd P case) shrinks as K increases. Consequentially, larger M would require lowering the sampling period for recovery based on a specific interval. This implies that in modulo undersampling, the sampling period should be optimized based on the recovery strategy (the exploited interval, and the parity of P).

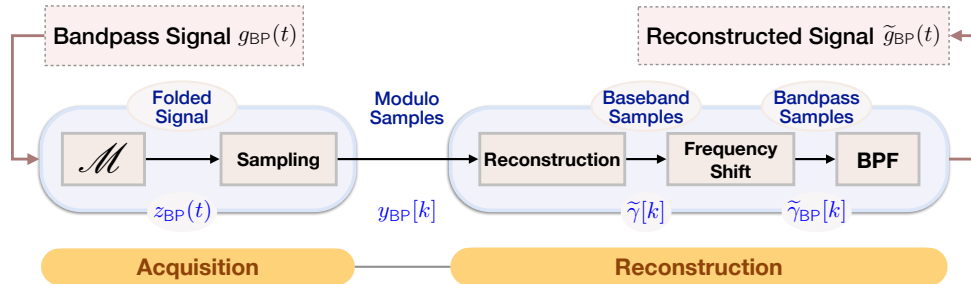


Fig. 6. Modulo bandpass acquisition and reconstruction pipeline.

Similarly to Corollary 1, the prevalence of AM signals and their spectral structure motivates the proof of the next corollary for non-ideal modulo bandpass sampling.

Corollary 2 (Fourier-Domain Recovery for AM Signals). *If $g_{\text{BP}}(t) \in \mathcal{B}_{(\Omega_L, \Omega_U)}$ is a τ -periodic function such that the side lobes of \hat{g} are symmetric, i.e., $\hat{g}(\Omega_L + \omega) = \hat{g}(\Omega_U - \omega)$, $\forall \omega \in [0, \Omega_{U,L}/2]$, then $g_{\text{BP}}(t)$ can be recovered from K modulo samples folded at most M times via Algorithm 2 if there exists $P_{\text{AM}} \in \mathbb{N}$ such that $\Omega_S = \frac{2\pi}{KT_S} = \frac{\Omega_U + \Omega_L}{2P_{\text{AM}}}$ and*

$$\Omega_{U,L} \leq \Omega_S \leq \frac{4\pi(Q_L - M - 1)}{\tau(2P_{\text{AM}} - 1)}. \quad (35)$$

Proof. Just as in Corollary 1, $\Omega_S = (\Omega_U + \Omega_L) / (2P_{\text{AM}})$ guarantees perfect overlapping of the spectral lobes. For recovery to work, we further require that $\Omega_{U,L} \leq \Omega_S$. Here, only the outer set $[Q_U^g + 1, K - Q_U^g - 2]$ can be used and hence, we require that $(K - 2Q_U^g - 2) \geq 2M$. Then, the RHS of (35) follows by substituting Q_U^g (28) (with $P = 2P_{\text{AM}}$) and $K = (\Omega_S \tau) / (2\pi)$. ■

IV. EXPERIMENTS

This section provides experiments that validate the theoretical results and demonstrate the potential of our modulo undersampling technique based on the sampling periods in Section III. We demonstrate computational demodulation and recovery of a bandpass signal from its modulo samples.

A. Numerical Simulations

As the most practical use case, we consider the case of baseband relocation. In the experiments, the bandwidth of the positive Fourier-domain coefficients is $\Omega_U - \Omega_L = \pi$, and their complex values are generated randomly so $\hat{g}_{\text{BP}}(\omega) = 100U_0 + j120U_1$, $\forall \omega \in [\Omega_L, \Omega_U]$, where $(U_0, U_1) \in (0, 1) \times (0, 1)$ are sampled from a uniform distribution. The negative Fourier-domain coefficients are the complex conjugate of the positive Fourier-domain coefficients. The bandpass signal is normalized so $\|g_{\text{BP}}\|_\infty = 1$. The experimental pipeline follows the block diagram in Fig. 6. The modulo of the bandpass signal, $z_{\text{BP}}(t)$ is sampled at period T_S for a time interval τ to produce a sequence of $K = \tau/T_S$ modulo samples $y_{\text{BP}}[k]$, and the samples that are recovered by Algorithm 1 and Algorithm 2 are denoted by $\tilde{\gamma}_{\text{BP}}^{\text{US}}[k]$ and $\tilde{\gamma}_{\text{BP}}^{\text{FP}}[k]$, respectively. Both algorithms recover the signal up to an additive constant of $2\lambda\mathbb{Z}$. This factor is estimated from the ground-truth samples $\gamma_{\text{BP}}[k]$, and the MSE between the signals is measured and denoted by $\mathcal{E}(\gamma_{\text{BP}}, \tilde{\gamma}_{\text{BP}}^{\text{US}})$ and $\mathcal{E}(\gamma_{\text{BP}}, \tilde{\gamma}_{\text{BP}}^{\text{FP}})$.

—• **Time-Domain Recovery.** The evaluation on this experiment is based on 1000 random realizations of a bandpass signal $g_{\text{BP}} \in \mathcal{B}_{(50\pi, 51\pi)}$ with $\lambda \sim \mathcal{U}(0.05, 0.1)$. According to (3), the sampling period should

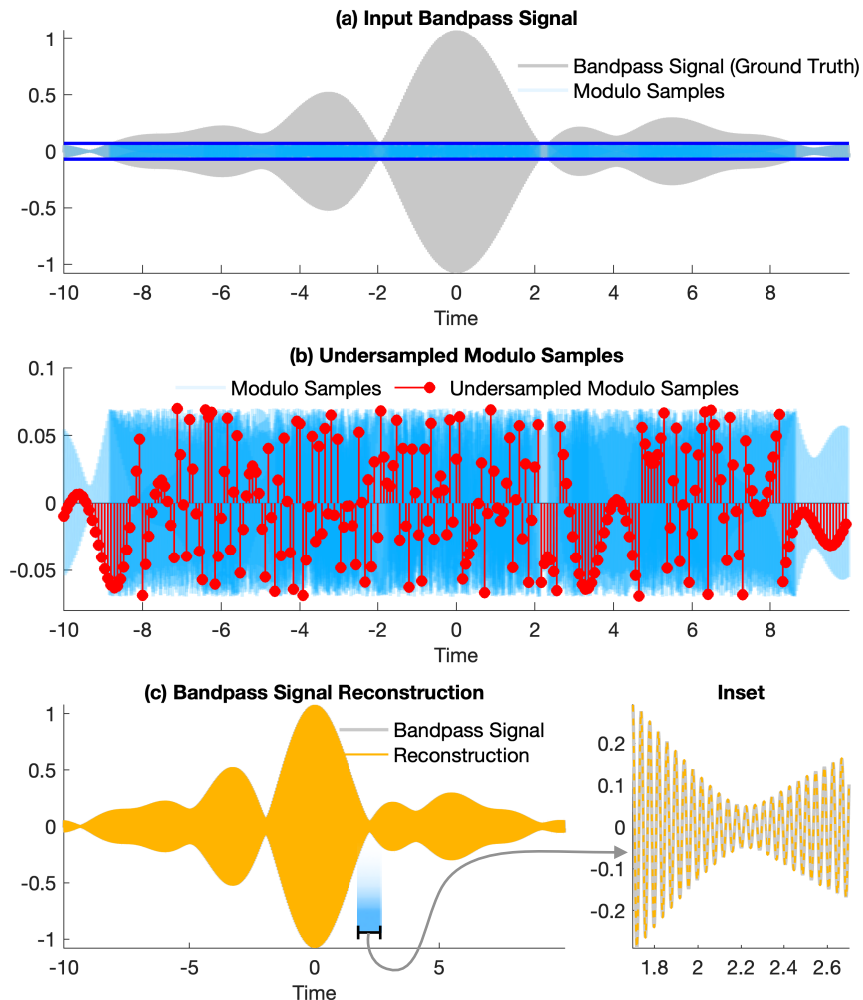


Fig. 7. Reconstruction of a bandpass signal with $\Omega_L = 50\pi, \Omega_U = 51\pi$ from its modulo samples at $T_S = 8 \times 10^{-2}$, where $\lambda = 0.07, P = 5$. Reconstruction with Algorithm 1 achieves $\mathcal{E}(\gamma_{BP}, \tilde{\gamma}_{BP}^{US}) = 2.06 \times 10^{-34}$.

satisfy $T_S \leq T_{US}^{BP} = 1/(102\pi e) \approx 1.1 \times 10^{-3}$. However, according to Theorem 1 with $P = 5$ recovery is still possible for $0.080 \leq T_S \leq 0.085$. We set $T_S = 0.080$ to achieve baseband relocation in (22). The maximal reconstruction error achieved by Algorithm 1 is $\mathcal{E}(\gamma_{BP}, \tilde{\gamma}_{BP}^{US}) = 8.54 \times 10^{-32}$. This verifies the validity of theorem 1, and shows a factor of $8\pi e$ reduction in the required sampling period for bandpass signals recovery. The modulo samples of $g_{BP}(t)$ with $\lambda = 0.07$ and the reconstruction using Algorithm 1 with $N = 3$ are shown in Fig. 7.

—• **Fourier-Domain Recovery.** To test the utility of our numerical algorithm, 1000 random realizations of the signal $g_{BP} \in \mathcal{B}_{(199\pi, 200\pi)}$ and $\lambda \sim \mathcal{U}(0.02, 0.1)$ were generated. The maximum number of detected folds was $M = 259$. Without undersampling, recovery of g_{BP} using the US-FP algorithm requires a sampling period smaller than 4.4×10^{-3} . Based on (30), we observe that with $P = 2$ the sampling period can be eased to $5.8 \times 10^{-3} \leq T_S \leq 10 \times 10^{-3}$. We set $T_S = 10 \times 10^{-3}$, which relocates the bandpass signal to a baseband position (22). The maximal reconstruction error using Algorithm 2 is $\mathcal{E}(\gamma_{BP}, \tilde{\gamma}_{BP}^{FP}) = 6.39 \times 10^{-32}$.

TABLE I
HARDWARE EXPERIMENTS—SUMMARY OF PARAMETERS AND PERFORMANCE

Exp.	Fig. No.	T_S (ms)	K	τ (ms)	Ω_L (rad/s)	Ω_U (rad/s)	ρ	A_M	Ω_M (rad/s)	θ_M (rad)	Ω_C (rad/s)	θ_C (rad)	$\mathcal{E}(\gamma, \tilde{\gamma})$
0	Fig. 2	2.5	24	59.8	2.29×10^3	2.73×10^3	2.49	-2.502	219.91	1.147	2.51×10^3	-0.17	1.7×10^{-3}
1	Fig. 8	10	30	299	584.33	672.30	3.77	3.72	43.98	2.644	628.31	-0.93	7.1×10^{-3}
2	Fig. 9	2.5	24	59.8	2.29×10^3	2.73×10^3	2.6	2.47	216	-1.57×10^{-2}	2.5×10^3	-1.57×10^{-2}	4.26×10^{-4}

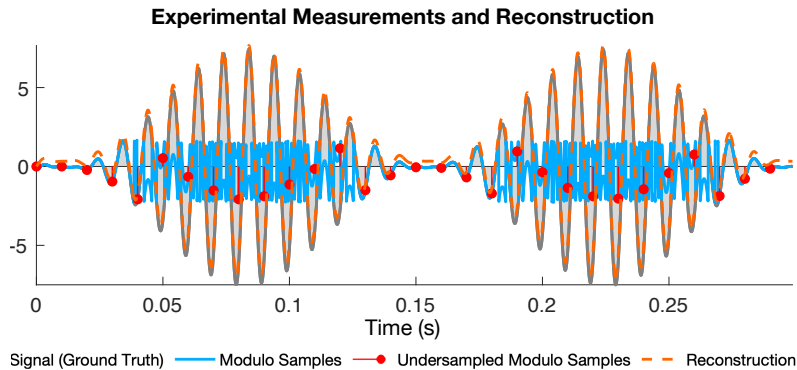


Fig. 8. Reconstruction from experimental data using \mathcal{M} -ADC. The experimental parameters are in Table I (Exp. 1).

B. Hardware Experiments

Experimental Protocol. The results for non-ideal modulo architectures can be validated via hardware experiments, by achieving computational demodulation and recovery of a bandpass signal from its modulo samples. The input signal follows,

$$g_{BP}(t) = A_M (1 + \cos(\Omega_M t + \theta_M)) \sin(\Omega_C t + \theta_C) \quad (36)$$

where $\{A_M, \Omega_M, \theta_M\}$ are the amplitude, frequency and phase of a message wave, and $\{\Omega_C, \theta_C\}$ are the frequency and phase of a carrier wave. The minimal and maximal frequencies of the bandpass signal in (36) are $\Omega_L = \Omega_C - \Omega_M$ and $\Omega_U = \Omega_C + \Omega_M$, respectively. In the experimental prototype, the signal (36) is generated by a TTI-TG5011 function generator, and then fed into the \mathcal{M} -ADC and a 4-channel DS0-X 3024A oscilloscope that simultaneously samples the input and the output of the \mathcal{M} -ADC to produce the ground-truth and the modulo samples. The sampling and reconstruction pipeline follows Fig. 6. For validation purposes, standard curve fitting techniques are used to estimate the parameters of (36).

Exp. 1: Reconstruction from Non-ideal Modulo Samples. To show demodulation and reconstruction using Algorithm 2, a signal with a period of $\tau = 299$ ms that obeys (36) with the parameters $A_M = 3.72$, $\Omega_M = 43.98$ rad/s, $\theta_M = 2.64$, $\Omega_C = 628.31 \times 10^3$ rad/s, and $\theta_C = -0.93 \times 10^{-2}$ rad is generated. The signal was fed into the \mathcal{M} -ADC with a threshold $\lambda \approx 2.01 \pm 3/20$, where $\pm 3/20$ is a manually adjustable design parameter, and then sampled at period $T_S = 10$ ms. The produced modulo samples $y[k]$ have $Q_U^g = 3$ and $M = 4$. As (36) is an AM signal, we validate that $\Omega_S = 2\pi/T_S = 200\pi$ rad/s satisfies (23) with $P_{AM} = 1$ and also satisfies (35) since $\Omega_{U,L} = 28\pi \leq 200\pi \leq 293\pi$. The conditions of Corollary 2 are satisfied so we can use Algorithm 2 with input $y[k]$, to produce the recovered samples $\tilde{\gamma}^{FP}[k]$. The error compared to the sequence $\gamma[k] = g(kT_S)$ is $\mathcal{E}(\gamma, \tilde{\gamma}^{FP}) = 7.1 \times 10^{-3}$, which verifies that $y_{BP}[k] \approx y[k]$ when undersampled. We then use interpolation with $\text{sinc}(\Omega_S t)$ to get $\tilde{g}^{FP}(t)$, and recover $\tilde{g}_{BP}(t) = \tilde{g}^{FP}(t) \frac{\sin(\Omega_C t + \theta_C)}{\sin \theta_C}$. The corresponding signals are shown in Fig. 8.

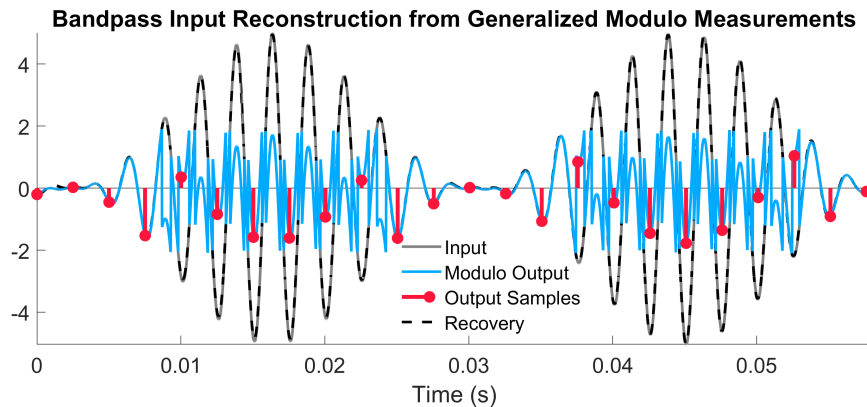


Fig. 9. Reconstruction from experimental data using the generalized \mathcal{M} -ADC. The experimental parameters are in Table I (Exp. 2).

Exp. 2: Reconstruction From Generalized Modulo Nonlinearity. The input is generated using (36) with $\Omega_M = 216$ rad/s, $\Omega_C = 2.5 \times 10^3$ rad/s, $\theta_M = \theta_C = -1.57 \times 10^{-2}$ rad, and $A_M = 2.47$. The generalized modulo nonlinearity parameters are $\lambda = 1.93$, $h = 0.88$, leading to a ratio $\rho = 2.6$ between the input amplitude and modulo threshold. The input is bandpass, satisfying $\{\Omega_L, \Omega_U\} = \{2.29, 2.73\} \times 10^3$. The input and output of the modulo were sampled with period $T_S = 2.5 \times 10^{-3}$, which is more than double the Nyquist sampling period of $T_{NS} = 1.2$ ms. This resulted in $K = 24$ samples. The input $g_{BP}(t)$, modulo output $z(t)$ and output samples $y[k] = z(kT_S)$ are depicted in Fig. 9. The samples of the baseband signal $g(kT_S)$ were subsequently recovered using Algorithm 1 with threshold λ_h . The signal $g(t)$ is reconstructed via interpolation with $\text{sinc}(\Omega t)$, where $\Omega = \frac{\pi}{T_S}$. The input $g_{BP}(t)$, recovered as $\tilde{g}_{BP}(t) = \tilde{g}(t) \frac{\sin(\Omega_C t + \theta_C)}{\sin \theta_C}$, is depicted in Fig. 9. The error between the recovered input and ground truth is $\mathcal{E}(\gamma_{BP}, \tilde{\gamma}_{BP}) = 4.26 \times 10^{-4}$.

V. CONCLUSIONS AND FUTURE WORK

In this paper, we proposed a computational sensing-based solution for the efficient acquisition of bandpass signals with a high dynamic range. Our approach is based on modulo folding architectures, whose distinct advantages had been previously proven for bandlimited signal types, but such advantages have not yet been capitalized for bandpass signals. In the sequel, we have shown that the characteristics of a bandpass input signal can be leveraged to allow a unique mapping between bandpass and modulo samples at sub-Nyquist rates. Based on that, we provided new sampling conditions guaranteeing recovery in the case bandpass and periodic bandpass signals. Considering the practicalities of modulo ADCs, we analyzed three different folding architectures, namely, the ideal modulo, non-ideal modulo and generalized modulo. Furthermore, feasible recovery algorithms that show that recovery is possible at the reported rates in both time- and frequency-domains are presented as well. Our numerical experiments validated the underlying theoretical findings. Taking a step closer to practice, we validated our algorithms with hardware experiments, thus establishing their practical advantages.

The main message of this work is that folding architectures are suitable for undersampling-based acquisition. Several real-life signal processing systems implement undersampling using ADCs but suffer from dynamic range limitations, thus creating a research gap; our work on the other hand shows its relevancy to a wide range of real-life signal processing systems.

—*Future Work*: The next step forward will be a study of the framework’s integration into different architectures that leverage bandpass sampling in hardware devices [39]–[41], and the challenges that arise in the context. This may include

- Multi-channel time-interleaved ADC, where the samples follow a non-uniform, periodic pattern and aliasing is present in the baseband signal as well [31].
- Sigma-Delta ADCs, where a feedback loop is utilized for noise shaping around a centered frequency [40].
- Software-defined radios, where algorithms are required to effectively filter and process multiple passbands.

APPENDIX

TABLE II
FREQUENTLY USED SYMBOLS

Symbol	Definition
$\mathbb{1}_{\mathcal{D}}(t)$	Indicator function on the domain \mathcal{D} .
\mathcal{M}_{λ}	Ideal modulo non-linearity with threshold λ .
$\widetilde{\mathcal{M}}_{\lambda}$	Non-ideal modulo non-linearity with threshold λ .
$\mathcal{M}_{\mathbf{H}}$	Generalized modulo operator with $\mathbf{H} = [\lambda, h, \alpha]$ where h is the hysteresis parameter and α is the transient duration.
$g_{\text{BP}}(t), g(t)$	Bandpass and corresponding bandlimited input signals.
$\Omega_{\text{S}}, T_{\text{S}}$	Sampling frequency (rad/s) and period $T_{\text{S}} = 2\pi/\Omega_{\text{S}}$ (s).
$\gamma[k], \gamma_{\text{BP}}[k]$	Input samples $\gamma_{\text{BP}}[k] = g_{\text{BP}}(kT_{\text{S}}), \gamma[k] = g(kT_{\text{S}})$.
$y[k], y_{\text{BP}}[k]$	Modulo samples of lowpass and bandpass functions.
$r[k], r_{\text{BP}}[k]$	Residual samples of lowpass and bandpass functions.
\underline{f}	First order difference, $\underline{f}[k] = \Delta f = f[k+1] - f[k]$.
$\Delta^N(\cdot)$	Finite difference operator of order N .
$\widehat{f}(\omega)$	Continuous-time Fourier transform (FT) of $f(t)$.
$\widehat{f}_{\delta}(\omega)$	Normalized Fourier series (FS) with coefficients $f[k]$.
$\widehat{f}[n]$	Discrete Fourier transform (DFT) of the sequence $f[k]$.
$\Omega_{\text{L}}, \Omega_{\text{U}}$	Minimum and maximum frequencies of a function.
$\Omega_{\text{U,L}}$	Passband bandwidth $\Omega_{\text{U,L}} = \Omega_{\text{U}} - \Omega_{\text{L}}$.
Ω_{U}^g	Bandwidth of baseband function g computed via (17).
$Q_{\text{L}}, Q_{\text{U}}, Q_{\text{U}}^g$	Indices for $\Omega_{\text{L}}, \Omega_{\text{U}}, \Omega_{\text{U}}^g$ on a discrete, normalized axis (27).
\mathcal{B}_{Ω}	Space of Ω -bandlimited functions.
$\mathcal{B}_{(\Omega_{\text{L}}, \Omega_{\text{U}})}$	Space of functions with spectrum inside $[\Omega_{\text{L}}, \Omega_{\text{U}}]$.
$\mathcal{E}(\mathbf{x}, \mathbf{y})$	Mean squared error between vectors \mathbf{x} and \mathbf{y} .

Notation. The sets of real, integer and natural numbers are denoted by $\mathbb{R}, \mathbb{Z}, \mathbb{N}$ respectively. We denote by $f(t), t \in \mathbb{R}$ continuous-time functions and by $f[k], k \in \mathbb{Z}$ discrete-time sequences. The p -norm for functions in $f \in L^p(\mathbb{R})$ is denoted as $\|f\|_p$, for $1 \leq p < \infty$. The Fourier series (FS) representation of a τ -periodic $f(t)$ is,

$$f(t) \stackrel{\text{def}}{=} \sum_{k \in \mathbb{Z}} f_k e^{-j \frac{2\pi}{\tau} tk}, \quad f_k = \frac{2\pi}{\tau} \int_{\tau/2}^{\tau/2} f(t) e^{j \frac{2\pi}{\tau} tk} dt.$$

The notation $\widehat{f}(\omega)$ is used for the Fourier transform of a continuous-time function $f(t) \in L^1(\mathbb{R})$. The sampled or discrete Fourier transform (DFT) of sequence $\{f[k]\}_{k=0}^{K-1}$ is $\widehat{f}[n] \stackrel{\text{def}}{=} \sum_{k=0}^{K-1} f[k] e^{-j\frac{2\pi}{K}kn}$. The Paley-Wiener class is denoted by PW_Ω , that is, $f \in \mathcal{B}_\Omega \cap L^2(\mathbb{R})$. The Dirac distribution is denoted $\delta(t)$. The first order difference sequence is defined as $\underline{f}[k] = (\Delta f)[k] = f[k+1] - f[k]$, and $(\Delta^N f)[k] = (\Delta(\Delta^{N-1} f))[k]$ is the N^{th} order difference sequence. The mean squared error (MSE) between $\mathbf{x}, \mathbf{y} \in \mathbb{R}^K$ is $\mathcal{E}(\mathbf{x}, \mathbf{y}) \stackrel{\text{def}}{=} \frac{1}{K} \sum_{k=0}^{K-1} |x[k] - y[k]|^2$.

REFERENCES

- [1] A. Bhandari, F. Kraemer, and R. Raskar, "On unlimited sampling," in *Intl. Conf. on Sampling Theory and Applications (SampTA)*, Jul. 2017.
- [2] —, "Methods and apparatus for modulo sampling and recovery," US Patent US10 651 865B2, May, 2020.
- [3] —, "On unlimited sampling and reconstruction," *IEEE Trans. Signal Process.*, vol. 69, pp. 3827–3839, Dec. 2020.
- [4] A. Bhandari, F. Kraemer, and T. Poskitt, "Unlimited sampling from theory to practice: Fourier-Prony recovery and prototype ADC," *IEEE Trans. Signal Process.*, vol. 70, pp. 1131–1141, Sep. 2021.
- [5] A. Bhandari, "Back in the US-SR: Unlimited sampling and sparse super-resolution with its hardware validation," *IEEE Signal Process. Lett.*, vol. 29, pp. 1047–1051, Mar. 2022.
- [6] D. Florescu and A. Bhandari, "Time encoding via unlimited sampling: Theory, algorithms and hardware validation," *IEEE Trans. Signal Process.*, vol. 70, pp. 4912–4924, Oct. 2022.
- [7] A. Bhandari, A. Kadambi, and R. Raskar, *Computational Imaging*, 1st ed. MIT Press, Oct. 2022, OA URL: <https://imagingtext.github.io/>.
- [8] A. Bhandari, F. Kraemer, and R. Raskar, "Unlimited sampling of sparse sinusoidal mixtures," in *IEEE Intl. Sym. on Information Theory (ISIT)*, Jun. 2018.
- [9] G. Shtendel and A. Bhandari, "HDR-ToF: HDR time-of-flight imaging via modulo acquisition," in *IEEE Intl. Conf. on Image Processing (ICIP)*, Oct. 2022, pp. 3808–3812.
- [10] A. Bhandari, "Unlimited sampling with sparse outliers: Experiments with impulsive and jump or reset noise," in *IEEE Intl. Conf. on Acoustics, Speech and Sig. Proc. (ICASSP)*, May 2022, pp. 5403–5407.
- [11] M. Beckmann, A. Bhandari, and F. Kraemer, "The modulo radon transform: Theory, algorithms, and applications," *SIAM Journal on Imaging Sciences*, vol. 15, no. 2, pp. 455–490, Apr. 2022.
- [12] Z. Liu, A. Bhandari, and B. Clerckx, " λ -MIMO: Massive MIMO via modulo sampling," Arxiv Preprint (arXiv:2210.10193), Oct. 2022.
- [13] D. Florescu, F. Kraemer, and A. Bhandari, "The surprising benefits of hysteresis in unlimited sampling: Theory, algorithms and experiments," *IEEE Trans. Signal Process.*, vol. 70, pp. 616–630, Jan. 2022.
- [14] D. Florescu and A. Bhandari, "Unlimited sampling via generalized thresholding," in *Intl. Sym. on Info. Theory (ISIT)*. IEEE, Jun. 2022.
- [15] —, "Unlimited sampling with local averages," in *IEEE Intl. Conf. on Acoustics, Speech and Signal Processing (ICASSP)*, May 2022, pp. 5742–5746.
- [16] —, "Modulo event-driven sampling: System identification and hardware experiments," in *IEEE Intl. Conf. on Acoustics, Speech and Signal Processing (ICASSP)*, May 2022, pp. 5747–5751.
- [17] D. Florescu, F. Kraemer, and A. Bhandari, "Event-driven modulo sampling," in *IEEE Intl. Conf. on Acoustics, Speech and Signal Processing (ICASSP)*, Jun. 2021.
- [18] O. Ordentlich, G. Tabak, P. K. Hanumolu, A. C. Singer, and G. W. Wornell, "A modulo-based architecture for analog-to-digital conversion," *IEEE J. Sel. Topics Signal Process.*, pp. 825–840, Aug. 2018.
- [19] E. Romanov and O. Ordentlich, "Above the Nyquist rate, modulo folding does not hurt," *IEEE Signal Process. Lett.*, vol. 26, no. 8, pp. 1167–1171, Aug. 2019.
- [20] S. Rudresh, A. Adiga, B. A. Shenoy, and C. S. Seelamantula, "Wavelet-based reconstruction for unlimited sampling," in *IEEE Intl. Conf. on Acoustics, Speech and Sig. Proc. (ICASSP)*, Apr. 2018, pp. 4584–4588.
- [21] O. Musa, P. Jung, and N. Goertz, "Generalized approximate message passing for unlimited sampling of sparse signals," in *IEEE Global Conf. on Sig. and Info. Proc. (GlobalSIP)*. IEEE, Nov. 2018.
- [22] D. Prasanna, C. Sriram, and C. R. Murthy, "On the identifiability of sparse vectors from modulo compressed sensing measurements," *IEEE Signal Process. Lett.*, vol. 28, pp. 131–134, Jan. 2021.

- [23] L. G. Ordonez, P. Ferrand, M. Duarte, M. Guillaud, and G. Yang, “On full-duplex radios with modulo-ADCs,” *IEEE Open Journal of the Communications Society*, vol. 2, pp. 1279–1297, Jun. 2021.
- [24] Y. Gong, L. Gan, and H. Liu, “Multi-channel modulo samplers constructed from gaussian integers,” *IEEE Signal Process. Lett.*, vol. 28, pp. 1828–1832, Aug. 2021.
- [25] E. Azar, S. Mulleti, and Y. C. Eldar, “Residual recovery algorithm for modulo sampling,” in *IEEE Intl. Conf. on Acoustics, Speech and Sig. Proc. (ICASSP)*. IEEE, May 2022.
- [26] A. Weiss, E. Huang, O. Ordentlich, and G. W. Wornell, “Blind modulo analog-to-digital conversion,” *IEEE Trans. Signal Process.*, vol. 70, pp. 4586–4601, Aug. 2022.
- [27] A. Bhandari and F. Kraemer, “HDR imaging from quantization noise,” in *IEEE Intl. Conf. on Image Processing (ICIP)*, Oct. 2020, pp. 101–105.
- [28] R. Guo and A. Bhandari, “ITER-SIS: Robust unlimited sampling via iterative signal sieving,” in *IEEE Intl. Conf. on Acoustics, Speech and Sig. Proc. (ICASSP)*, Jun. 2023.
- [29] J. L. Brown, “On uniform sampling of amplitude modulated signals,” *IEEE Trans. Aerosp. Electron. Syst.*, vol. AES-19, no. 4, pp. 633–635, Jul. 1983.
- [30] R. Vaughan, N. Scott, and D. White, “The theory of bandpass sampling,” *IEEE Trans. Signal Process.*, vol. 39, no. 9, pp. 1973–1984, Sep. 1991.
- [31] M. Wahab and B. C. Levy, “Direct complex envelope sampling of bandpass signals with m-channel time-interleaved ADCs,” *IEEE Trans. Signal Process.*, vol. 70, pp. 4804–4819, Oct. 2022.
- [32] O. D. Grace and S. P. Piti, “Quadrature sampling of high-frequency waveforms,” *The Journal of the Acoustical Society of America*, vol. 44, no. 5, pp. 1453–1454, Nov. 1968.
- [33] W. Knight, R. Pridham, and S. Kay, “Digital signal processing for sonar,” *Proc. IEEE*, vol. 69, no. 11, pp. 1451–1506, Nov. 1981.
- [34] W. Waters and B. Jarrett, “Bandpass signal sampling and coherent detection,” *IEEE Trans. Aerosp. Electron. Syst.*, vol. AES-18, no. 6, pp. 731–736, Nov. 1982.
- [35] D. Rice and K. Wu, “Quadrature sampling with high dynamic range,” *IEEE Trans. Aerosp. Electron. Syst.*, vol. AES-18, no. 6, pp. 736–739, Nov. 1982.
- [36] J. Kang, H. Yoon, C. Yoon, and S. Y. Emelianov, “High-frequency ultrasound imaging with sub-Nyquist sampling,” *IEEE Trans. Ultrason., Ferroelectr., Freq. Control*, vol. 69, no. 6, pp. 2001–2009, Jun. 2022.
- [37] A. Hirabayashi, H. Ogawa, and K. Kitagawa, “Fast surface profiler by white-light interferometry by use of a new algorithm based on sampling theory,” *Applied Optics*, vol. 41, no. 23, p. 4876, Aug. 2002.
- [38] K. G. Larkin, “Efficient nonlinear algorithm for envelope detection in white light interferometry,” *Journal of the Optical Society of America A*, vol. 13, no. 4, p. 832, Apr. 1996.
- [39] C. Fazi and P. G. Neudeck, “Wide dynamic range RF mixers using wide-bandgap semiconductors,” in *IEEE MTT-S International Microwave Symposium Digest*. IEEE, Jun. 1997.
- [40] M. S. Kappes, “A 2.2-mW CMOS bandpass continuous-time multibit Δ - Σ ADC with 68 dB of dynamic range and 1-MHz bandwidth for wireless applications,” *IEEE J. Solid-State Circuits*, vol. 38, no. 7, Jul. 2003.
- [41] H.-M. Seo, C.-G. Woo, and P. Choi, “Relationship between ADC performance and requirements of digital-IF receiver for WCDMA base-station,” *IEEE Trans. Veh. Technol.*, vol. 52, no. 5, pp. 1398–1408, Sep. 2003.
- [42] T. Feuillen, M. Alae-Kerahroodi, A. Bhandari, M. R. B. Shankar, and B. Ottersten, “Unlimited sampling for FMCW radars: A proof of concept,” in *IEEE Radar Conf. (RadarConf22)*, Mar. 2022.
- [43] T. Feuillen, M. R. B. Shankar, and A. Bhandari, “Unlimited sampling radar: Life below the quantization noise,” in *IEEE Intl. Conf. on Acoustics, Speech and Sig. Proc. (ICASSP)*. IEEE, Jun. 2023.
- [44] M. B. Pursley, “Analog communications,” in *Reference Data for Engineers*. Elsevier, 2002, pp. 23–1–23–19.